Korgesaar, Mihkel; Romanoff, Jani; Remes, Heikki

Influence of material non-linearity on load carrying mechanism and strain path in stiffened panel

Published in:
Procedia Structural Integrity

DOI:
10.1016/j.prostr.2017.07.050

Published: 01/01/2017

Document Version
Publisher's PDF, also known as Version of record

Please cite the original version:
Korgesaar, M., Romanoff, J., & Remes, H. (2017). Influence of material non-linearity on load carrying mechanism and strain path in stiffened panel. *Procedia Structural Integrity*, *5*, 713-720.
https://doi.org/10.1016/j.prostr.2017.07.050

Available online at www.sciencedirect.com

ScienceDirect

Procedia Structural Integrity 5 (2017) 713–720

Structural Integrity Procedia

www.elsevier.com/locate/procedia

2nd International Conference on Structural Integrity, ICSI 2017, 4-7 September 2017, Funchal, Madeira, Portugal

Influence of material non-linearity on load carrying mechanism and strain path in stiffened panel

Mihkel Kõrgesaar[a]*, Jani Romanoff[a], Heikki Remes[a]

[a]*Aalto University, Department of Mechanical Engineering, Puumiehenkuja 5a, 00076 Aalto, Espoo, Finland*

Abstract

This paper investigates the influence of material non-linearity on load carrying mechanism and strain path in stiffened panel. First, clamped stiffened panel with dimensions of 1.2 x 1.2 m was penetrated with rigid indenter until fracture took place. Second, panel material was characterized with standard tensile tests using flat test coupons extracted from the face sheet of the panel. Failure strain for different element lengths was calibrated using iterative state-of-the-art procedure. Numerical finite element simulations were performed using failure strain calibrated with tensile tests. Comparison of numerical and experimental force-displacement curves of panel clearly shows that this widely used approach is not sufficient for reliable element size independent numerical simulations. The reason is that failure strain scaling depends on the element size as well as stress state. The stress state in the structural component however, can considerably vary from that observed in tensile test.

Peer-review under responsibility of the Scientific Committee of ICSI 2017

Keywords: Type your keywords here, separated by semicolons ;

1. Introduction

A reliable consideration of material non-linearity and failure strain in crashworthiness analysis of large complex structures such as ship is a challenge with an increasing importance in the last decades. Ship collisions, groundings and penetration of objects through the shell plating of the ship can lead to loss of ship buoyancy and consequent

* Corresponding author. Tel.: +37253439557
E-mail address: Mihkel.korgesaar@aalto.fi

2452-3216
Peer-review under responsibility of the Scientific Committee of ICSI 2017
10.1016/j.prostr.2017.07.050

progressive flooding. The size and location of the opening defines the seriousness of the incident and thus, also the extent of the final damage. Therefore, prediction of the opening size has fundamental importance in ship safety assessment especially in regions with high traffic. In this respect, non-linear finite element simulations including ductile fracture have become a standard design tool to predict structural response for accidental loads. As the simulated structures are large, ductile fracture must be resolved with plane stress structural shell elements where element length is orders of magnitude higher than micro-scale fracture process. Moreover, ductile fracture in metals is preceded by localization of strains, i.e. necking, that makes the finite element solution mesh size dependent if no special strain gradient dependent plasticity theories are adopted (Mikkelsen, 1997). Consequently, the governing challenge in fracture modelling of large structures simplifies to correctly describing the post-necking behavior of material until point of fracture initiation with large shell elements, or in other words, *upscaling* the material behavior from simple coupon tests to large structural shell elements, see the illustration in Fig. 1a.

In general, the fracture modelling approaches adopted in the ship collision and grounding analyzes can be separated into two categories: coupled and uncoupled. In coupled approaches fracture is modelled as a process of damage accumulation within continuum, hence the coupling of constitutive model and fracture model (AbuBakar and Dow, 2013; Woelke and Abboud, 2012; Kõrgesaar and Romanoff, 2014). In the second approach fracture is considered as a sudden event when the stress or strain states of the undamaged continuum reach a critical level, beyond which element is considered as failed and removed from the analysis. The latter approach is more common in the analysis of ship structures and thus, is also adopted here. In this context one of the key parameters is the element failure strain. The term "element failure strain" is pertinent to analysis of large structures where element size acts as an averaging window for local strains that exhibit gradients dependent on the amount of necking. Commonly, the failure strain for different element lengths is determined using hybrid numerical-experimental approach (Simonsen and Lauridsen, 2000; Alsos et al., 2009). First, the standard tensile test with a dog-bone specimen is conducted where the load and displacement are recorded. Thereafter, tensile test is simulated with different element lengths, whereas failure strain for each element size is iteratively changed to capture the experimental fracture initiation point. The logarithmic relation fitted to the data is called Barba's law which is then extrapolated and used in the crash analysis of large structures. As shown in Fig. 1b, the observed relatively strong mesh size dependence arises due to combination of diffuse and localized necking.

Although this approach is widely used, there is still limited understanding of the influence of the used simplifications, e.g., the difference in strain path between tensile test and real structure on fracture prediction. In order to get deeper insight to these differences, this paper presents initial results on the influence of material-non linearity on load-carrying mechanics and strain-path in stiffened panel commonly used in ship side structure. Therefore, the approach mentioned above is used to simulate the failure in stiffened panel under quasi-static indentation. The key challenges in used approach are discussed.

2. Experiments and methods

2.1. Uniaxial tension test and simulations

Material of the tested stiffened panel is a standard structural steel S235JR commonly used in shipbuilding. To characterize the material behavior quasi-static tensile tests were performed with 3 mm thick dog-bone specimens (see Fig. 2b) using a 100 kN MTS servo-hydraulic universal testing machine. Test matrix is shown in Table 1. The loading speed was 2 mm/min. During testing, the force and displacement were recorded and these are shown in Fig. 2(a).

The equivalent stress - equivalent plastic strain curve was determined with iterative numerical approach; for results see Table 2. Material parameters were modified in the numerical finite element (FE) simulation until adequate correspondence was reached with measured force-displacement curve (see e.g. Dunand and Mohr, 2010; Luo and Wierzbicki, 2010). The elastic properties of the materials were described by a Young's modulus of E = 200 GPa, Poisson ratio of $\nu = 0.3$, and density of 7850 kg/m^3. von Mises yield criterion was used in the simulations assuming associated plastic flow and isotropic hardening. Strain hardening was described by a three-term Voce (1948) type of saturation model with yield stress of σ_0 and hardening parameters Q_i, C_i (i = 1~3) and n, see Table 2:

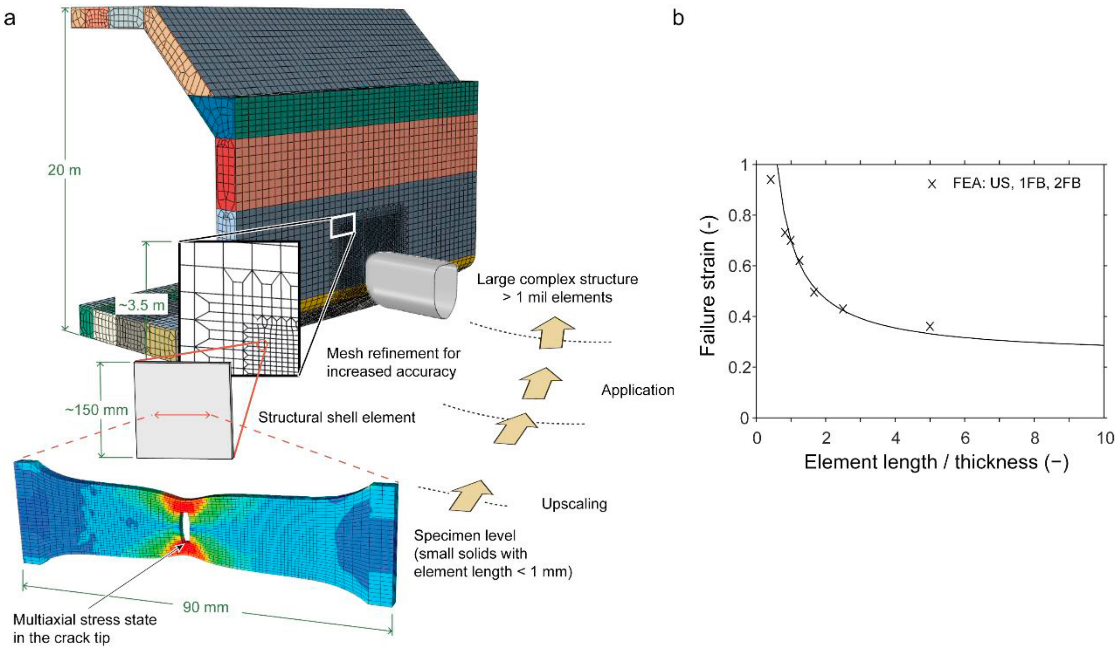

Fig. 1. (a) Depiction of the governing challenge in ductile fracture modelling of large structures. (b) Failure strain dependency determined with tensile test. Data from Alsos et al. (2009).

$$\bar{\sigma}=\left(\sigma_0+\sum_{i=1}^{3}Q_i\left(1-\exp\left(-C_i\left(\bar{\varepsilon}+\varepsilon_0\right)\right)\right)\right)\cdot\left(1+\bar{\varepsilon}\right)^n \quad (1)$$

where $\bar{\sigma}$ is the equivalent stress, $\bar{\varepsilon}$ is the equivalent plastic strain, and ε_0 accounts for the existence of a strain plateau. Numerical finite element simulations of the dog-bone tests were performed with FE software Abaqus 6.13-3/Explicit using reduced integration solid elements (C3D8R). In-plane element size in the gauge region was 0.3 x 0.3 with 4 elements through thickness. In developing the FE models, 1/8-symmetry of the specimen geometry and loading was exploited, see Fig.2 (c). The computational time in simulations was reduced by mass scaling the entire model in the beginning of the analysis by a factor of 14. Despite this large factor, comparison with non-mass scaled solution indicated that changes in the mass and consequent increases in the inertial forces did not alter the solution accuracy nor did it increase the kinetic energy over 5% of total internal energy. The force-displacement curve obtained from simulations is compared with experimental response in Fig. 2(a). Shell element calibration is described later in the simulations chapter.

Table 1. Description of tensile tests.

Specimen id.	t1 (mm)	t2(mm)	t (average)	Gauge width (mm)	Loading speed (mm/min)
DB-1-3	2.98	2.98	2.98	15.08	2
DB-2-3	3.00	2.97	2.99	15.04	2

Table 2. Material parameters for the hardening model

Thickness	σ_0 [MPa]	Q_1 [MPa]	Q_2 [MPa]	Q_3 [MPa]	C_1 [-]	C_2 [-]	C_3 [-]	ε_0 [-]	n
3 mm	280	84.32	470.1	137.8	25	0.6	1.454	-0.009	0.18

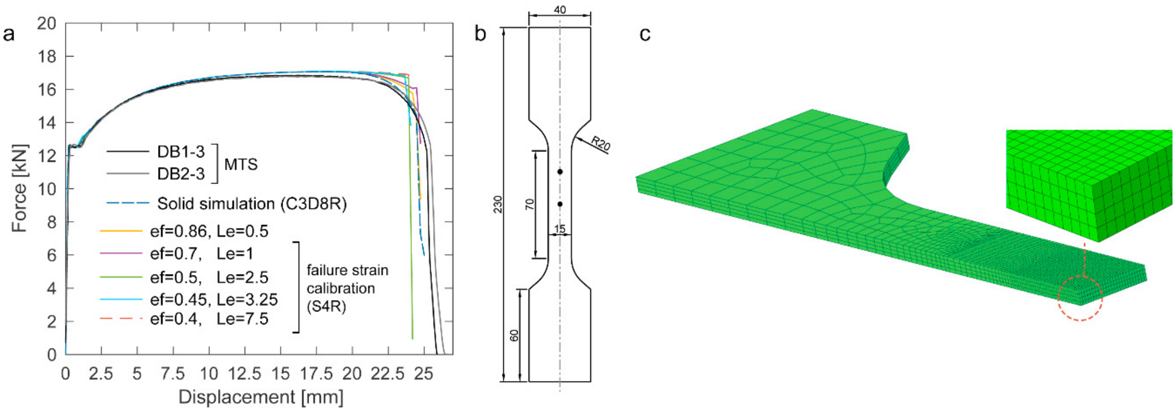

Fig. 2. Standard tensile testing. (a) Measured force-displacement compared with simulation results. (b) Geometry of the test coupon. The approximate location of the thickness measurements is indicated with black round marker. (c) Finite solid element model of the specimen.

2.2. Stiffened panel test

As part of the larger experimental test program quasi-static indentation experiments were performed to study force-indentation response and fracture behavior of stiffened steel and sandwich panels, for details see Kõrgesaar et al. (2016). For brevity, only the response of single stiffened panel test (from total of three tests) is discussed in this paper, justified by the excellent repeatability of the tests in terms of force-displacement response. Panels consisted of face plates reinforced with steel stiffeners welded together with laser stake welds, see Fig. 3. Ductility of the welds was confirmed by material hardness measurements in accordance with DNV-GL standards (Kõrgesaar et al., 2016).

Test set-up used in experiments is shown in Fig. 3(b). The panels were positioned between clamping (30 mm thick) and back support plates (40 mm) with total of 62 bolts – the bolt hole arrangement is shown in Fig.3(a). Clamping width in all edges was 120 mm, leaving unsupported span of square plate to be 0.96m. Both, top and bottom support

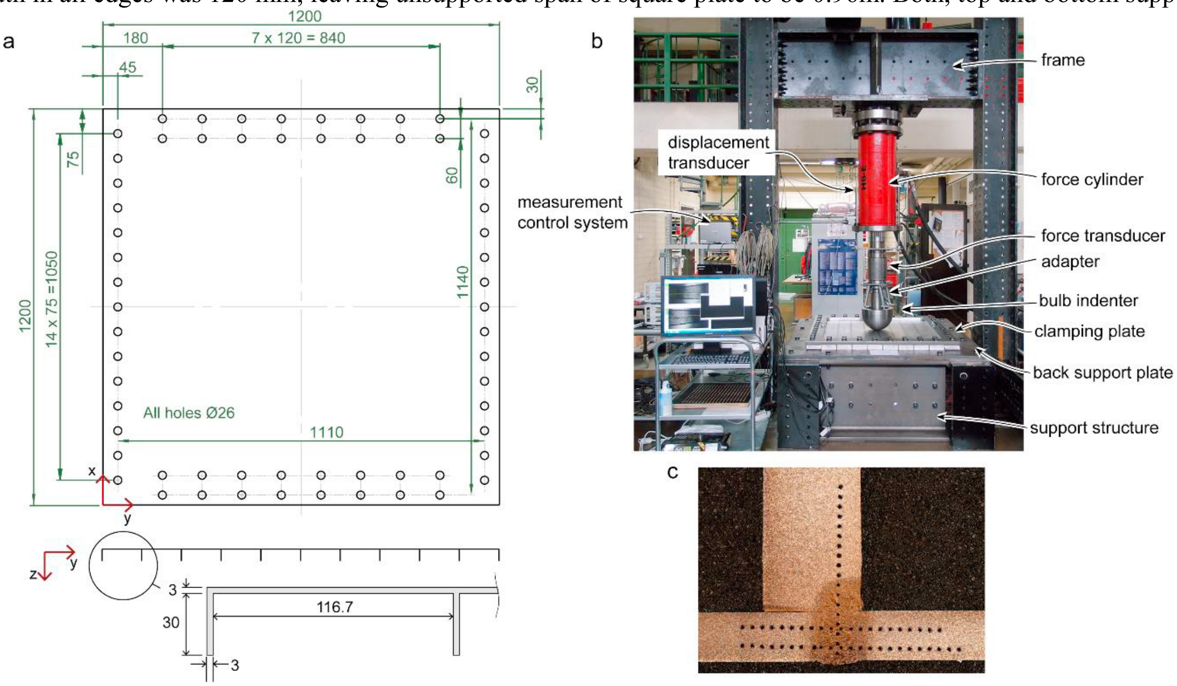

Fig. 3. (a) Dimensions in mm and geometry of the stiffened panel. (b) Experimental set-up. (c) Picture of the laser weld after hardness measurements.

plate were made from S355 structural steel. Bolts were fastened to torque of 800Nm. Calculated clamping force achieved was ~9 MN. The assembly was fixed to the support structure built from European wide flange I-beams (DIN 1025/EN 10034 HE600B) fastened together with grade 8.8 M24 steel bolts using four corner brackets. The clearance between panel and ground was 640 mm. To avoid stiffener buckling in the clamped region under the clamping plate steel inserts were used as supports.

The loading speed in tests was 10 mm/min. The force was generated with the hydraulic cylinder with maximum capacity of 1 MN. Applied indentation force was measured with 1MN force transducer connected to bottom end of the force cylinder. Indenter displacement was measured with HBM WA500 displacement transducer mounted between piston and cylinder. Bulb indenter was mounted on force transducer using adapter in between. Indenter had a polished surface finish, so friction coefficient in panel face – indenter interface could be in the range of 0.2-0.3 characterizing steel-to-steel contact. Indenter could rotate during indentation to protect force sensor from bending moments. Four springs were installed between indenter and force sensor to prevent movement of indenter in unloaded position. These springs were enough to suppress the indenter rotations before fracture initiation and even during early stage of fracture propagation.

3. Simulations

3.1. Element length dependent failure strain

Element length dependent failure strain is determined using shell element simulations, e.g. Simonsen and Lauridsen (2000). The tensile specimen was discretized using four different mesh densities in the gauge section with element length of L_e = 1, 2.5, 3.75 and 7.5 mm. Only symmetry along the longitudinal axis was exploited to exactly control the element length in the middle of the gauge section, see Fig. 4. Left edge of the specimen was clamped while velocity was applied on the right edge of the model. Failure strain in simulations was modified until correspondence was reached with measured force-displacement curve – the calibration results are shown in Fig. 2a.

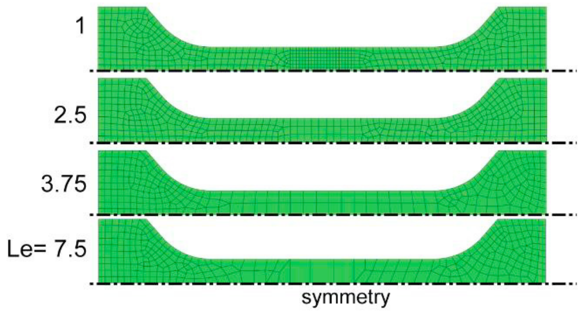

Fig. 4. Shell element models for failure strain determination. Units in mm.

3.2. Failure criterion

To simulate ductile fracture in stiffened panel we employ Cockcroft-Latham (CL) criterion (Cockcroft and Latham, 1968). The criterion is chosen as it is convenient to calibrate only based on the failure strain determined with tensile test in the previous Section. According to CL criterion failure occurs when integral of the maximum principal stress along the plastic strain path reaches a critical value. Wierzbicki and Werner (1998) showed that the CL criterion can be expressed as a function of stress triaxiality ($\eta = \sigma_h/\bar{\sigma}$, mean stress divided by equivalent von Mises stress) – this formulation is adopted herein. The criterion is implemented in the ABAQUS VUMAT subroutine through damage D indicator framework whereby element is removed from simulation once integral of the CL criterion along the plastic strain path reaches a critical value of 1. The damage in the element is given as

$$D=\frac{1}{\bar{\varepsilon}_f}\int 2\frac{1+\eta\sqrt{12-27\eta^2}}{3\eta+\sqrt{12-27\eta^2}}d\bar{\varepsilon}\le 1 \tag{2}$$

where $\bar{\varepsilon}_f$ is the failure strain determined with uniaxial tension test.

3.3. Panel simulations

Simulations were run using Abaqus/Explicit version 6.13-3 using reduced integration shell elements (S4R) with default hourglass control and 5 through thickness integration points. Figure 5 illustrates the set-up of the numerical model. Contact between different objects was modelled with general contact algorithm by defining rigid objects as masters. Contact definition included model for tangential and normal behavior. Tangential behavior between surfaces was modeled with penalty type friction formulation with friction coefficient of 0.25. The indentation experiment was simulated by assigning a constant vertical velocity of 1 m/s to the indenter, while constraining all other degrees of freedoms. Mass of the entire model was scaled in the beginning of the analysis by a factor of 14. Model was discretized with three different element densities at the fracture location, L_e = 1, 2.5, 3.75 and 7.5 mm. In rest of the model element size ranged from 10 to 15 mm.

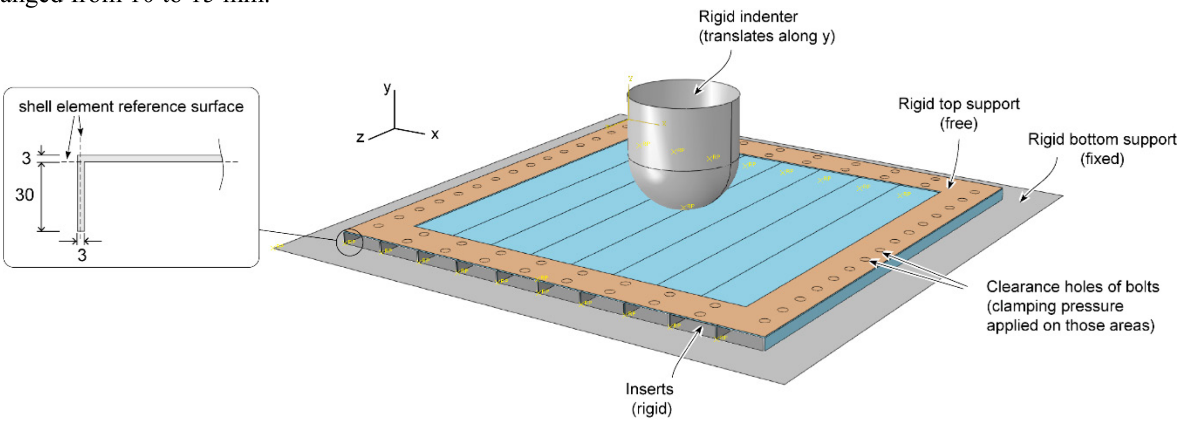

Fig. 5. FE model set-up.

4. Results

4.1. Load-response

Comparison of measured and simulated force-displacement (F-d) curves and the development of the strain path in failing elements is given in Fig. 6. Fig. 7 shows the failed panel at the end of the simulation. Scatter in F-d curves suggests that failure strain calibration based on uniaxial tension test is not sufficient. While 2.5 mm mesh captures the experimental response, this knowledge would be of little use in a “blind” test where experimental results are not available. The reason for observed sensitivity is the stress state difference between panel and tensile coupon at failure as shown in Fig.6b. Failure in the stiffened panel face plate takes place under equi-biaxial tension (BAT, $\eta = 2/3$) and plane strain (PST, $\eta = 1/\sqrt{3}$) (black and dark blue dots). In contrast, the strain path in critical element of the tensile test (orange color) corresponds to uniaxial tension (UAT, $\eta = 1/3$). Although stiffener fails also under uniaxial tension this happens once the load has already dropped down, thus the peak load in the F-d curve is governed by the fracture initiation in the plate. Recall, that in uniaxial tension the relatively strong mesh size dependence arises because of the combination of diffuse and localized necking, whereas in plane strain tension only localized neck develops and in equi-biaxial tension material localization is further delayed (Kõrgesaar et al., 2014; Walters, 2014). The failure in the panel however takes place exactly under these stress states as shown in Fig. 6 b that explains the scatter in results. Therefore, scaling the failure strain (fracture criterion) only based on uniaxial tension test without accounting the stress state in calibration leads to mesh sensitive results if the stress state is different in the structural component to be simulated.

Moreover, fracture morphology in Fig. 7 is affected by the accuracy of the simulation. Experimental F-d curve was most accurately captured by 2.5 and 3.75 mm mesh and the fracture path of these two cases are very similar as well as consistent with experimental fracture path. In analysis with 1 mm model the location of initiation is correct, but fracture propagates symmetrically to middle stiffener that was not observed in the test. In 7.5 mm model fracture initiates next to the middle stiffener and propagates along the stiffener before the second, perpendicular crack develops forming the final shape shown in Fig. 7.

Fig.8 shows the membrane stresses in the panel edges to illustrate the load-carrying mechanism of the panels. The comparison of normal stress along the clamped edge just prior to failure between 1, 2.5 and 7.5 mm solution suggests that inaccuracies in F-d curve have minor effect on the load carrying mechanism. The stress level at the panel edge gives also an indication of stress state in the panel. This is an important perspective towards failure simulations in conceptual design stage where response is approximated with elements that smear the response of plate and stiffener together. The stress state in panel is closer to uniaxial tension as opposed to equi-biaxial tension locally at the crack tip. This is due to the 23% higher cross-sectional area in the stiffener direction than opposite direction. Since stresses were acquired only along the edge of plate excluding stiffeners, it is rather interesting to observe how stiffeners guide the stress flow also in the plate.

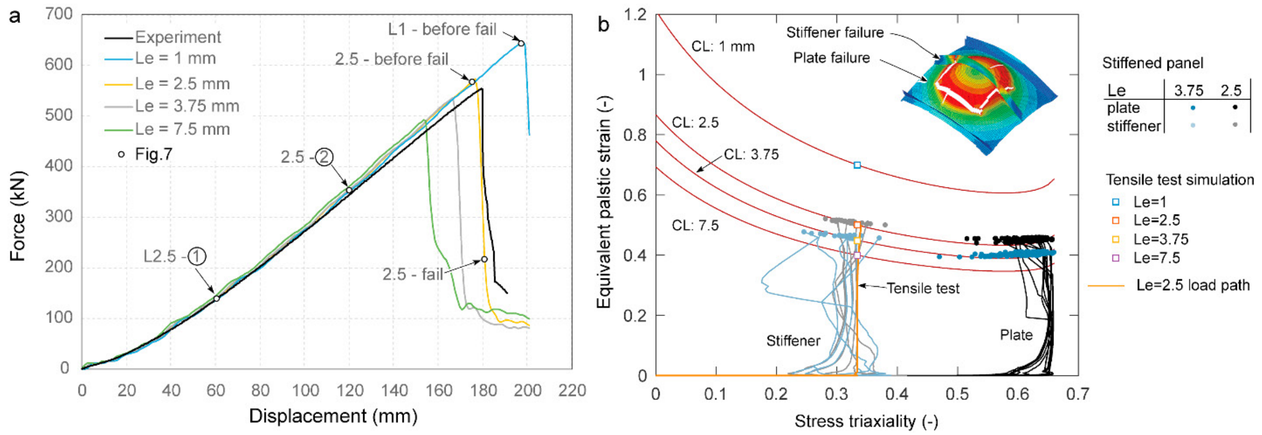

Fig. 6. (a) Measured force-displacement behavior of stiffened panel compared with simulation results. (b) Loading paths at the critical material points of the panel.

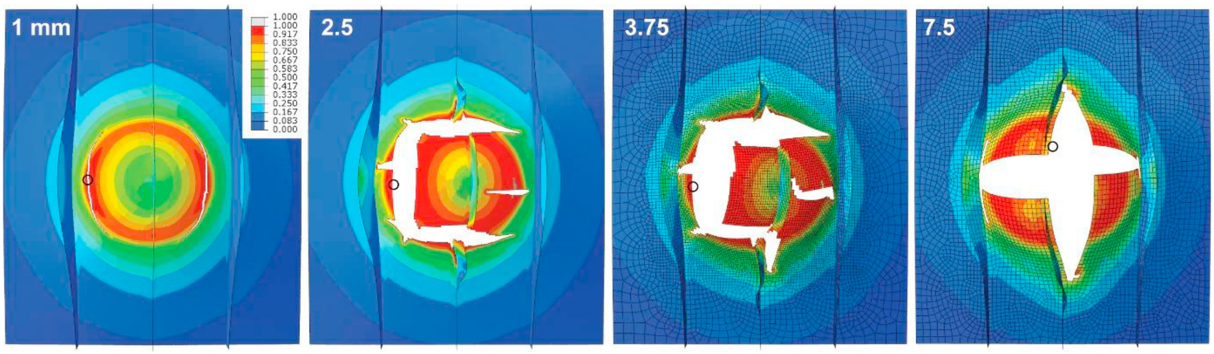

Fig. 7. Fracture path at the end of the simulation (same indenter displacement). Color contours show the damage in elements. The approximate location of fracture initiation is indicated with black circle.

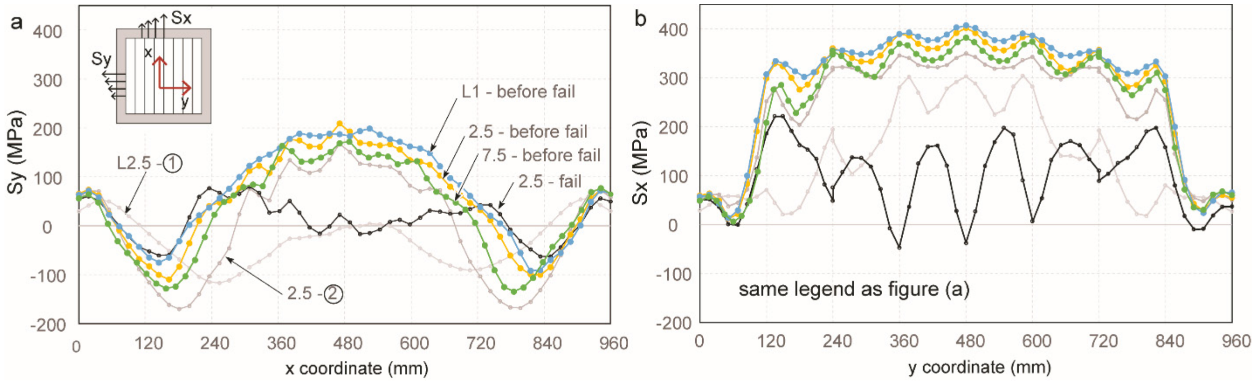

Fig. 8. Comparison of membrane stress normal to the panel edge (only plate) along the clamping line. (a) Along the left edge parallel to stiffener. (b) Along the top edge transverse to stiffener.

5. Conclusions

The paper investigated the influence of material non-linearity on load carrying mechanism and strain path in stiffened panel. Clamped stiffened panel was penetrated with rigid indenter until fracture took place. Panel material was characterized with standard tensile tests using flat test coupons extracted from the face sheet of the panel. Failure strain for different element lengths was calibrated using iterative state-of-the-art procedure. Numerical finite element simulations were performed using failure strain calibrated with tensile tests. Comparison of numerical and experimental force-displacement curves clearly shows that the approach is not sufficient for reliable element size independent numerical simulations as failure strain scaling depends on both, element size and stress state. Stress state at failure in tensile test corresponds to uniaxial tension, while in stiffened panel it varies between equi-biaxial and plane strain tension. Furthermore, element strain paths indicate that stress state can change during the loading history. How to account this in a reliable manner in damage indicator framework is subject of the future work.

6. References

Abubakar, A., Dow, R.S., 2013. International Journal of Solids and Structures Simulation of ship grounding damage using the finite element method. Int. J. Solids Struct. 50, 623–636. doi:10.1016/j.ijsolstr.2012.10.016

Alsos, H.S., Amdahl, J., Hopperstad, O.S., 2009. On the resistance to penetration of stiffened plates, Part II: Numerical analysis. Int. J. Impact Eng. 36, 875–887. doi:10.1016/j.ijimpeng.2008.11.004

Cockcroft, M.G., Latham, D.J., 1968. Ductility and the workability of Metals. J. Inst. Met. 96, 33–39. doi:citeulike-article-id:4789874

Dunand, M., Mohr, D., 2010. Hybrid experimental-numerical analysis of basic ductile fracture experiments for sheet metals. Int. J. Solids Struct. 47, 1130–1143. doi:10.1016/j.ijsolstr.2009.12.011

Kõrgesaar, M., Romanoff, J., 2014. Influence of mesh size, stress triaxiality and damage induced softening on ductile fracture of large-scale shell structures. Mar. Struct. 38, 1–17. doi:10.1016/j.marstruc.2014.05.001

Kõrgesaar, M., Romanoff, J., Palokangas, P., 2016. Penetration resistance of stiffened and web-core sandwich panels: experiments and simulations. Aalto University publication series SCIENCE + TECHNOLOGY; 12/2016, Aalto University, http://urn.fi/URN:ISBN:978-952-60-7187-9

Kõrgesaar, M., Remes, H., Romanoff, J., 2014. Size dependent response of large shell elements under in-plane tensile loading. Int. J. Solids Struct. 1–10. doi:10.1016/j.ijsolstr.2014.07.012

Luo, M., Wierzbicki, T., 2010. Numerical failure analysis of a stretch-bending test on dual-phase steel sheets using a phenomenological fracture model. Int. J. Solids Struct. 47, 3084–3102. doi:10.1016/j.ijsolstr.2010.07.010

Simonsen, B.C., Lauridsen, L.P., 2000. Energy absorption and ductile failure in metal sheets under lateral indentation by a sphere. Int. J. Impact Eng. 24, 1017–1039.

Voce E. The relationship between stress and strain for homogenous deformation. J Inst Met 1948;74:536–62.

Walters, C.L., 2014. Framework for adjusting for both stress triaxiality and mesh size effect for failure of metals in shell structures. Int. J. Crashworthiness 19, 1–12. doi:10.1080/13588265.2013.825366

Wierzbicki, T. and Werner, H. (1998), Cockcroft and Latham Revisited - Impact and Crashworthiness Laboratory Report Nr. 16, Technical report, MIT.

Woelke, P.B., Abboud, N.N., 2012. Modeling fracture in large scale shell structures. J. Mech. Phys. Solids 60, 2044–2063. doi:10.1016/j.jmps.2012.07.001